Draft version September 20, 2016
Preprint typeset using LaTeX style emulateapj v. 5/2/11

arXiv:1608.03707v2 [astro-ph.CO] 19 Sep 2016

ABS: AN ANALYTICAL METHOD OF BLIND SEPARATION OF CMB B-MODE FROM FOREGROUNDS

Pengjie Zhang, Jun Zhang, Le Zhang
Center for Astronomy and Astrophysics, Department of Physics and Astronomy, Shanghai Jiao Tong University, 955 Jianchuan road, Shanghai, 200240

Draft version September 20, 2016

ABSTRACT

Extracting CMB B-mode polarization from complicated foregrounds is a challenging task in searching for inflationary gravitational waves. We propose an analytical solution to the B-mode power spectrum measurement directly from post-processing the cross bandpower between different frequency bands, without free parameters or fitting procedures, or any assumptions on foregrounds. Testing against a variety of foregrounds, survey frequency configurations and instrument noise, we verify its applicability and numerical stability. It also provides a clean diagnostic for future experiments to achieve unbiased B-mode measurement. Furthermore, it has applications beyond CMB and can even have profound impacts in totally different areas such as cosmic magnification.

Subject headings: Cosmology: inflation

1. INTRODUCTION

Searching for inflationary gravitational waves (Starobinskiĭ 1979) through the induced CMB B-mode polarization (Seljak & Zaldarriaga 1997; Seljak 1997; Kamionkowski et al. 1997) is a major endeavour of cosmology (e.g. BICEP: BICEP2 Collaboration et al. (2014); Grayson et al. (2016); BICEP2/Keck and Planck Collaborations et al. (2015); ACTpol: Thornton et al. (2016); SPTpol: Keisler et al. (2015); POLARBEAR: Inoue et al. (2016); PIPER: Gandilo et al. (2016); COrE: The COrE Collaboration et al. (2011); EPIC: Bock et al. (2008); LiteBIRD: Matsumura et al. (2014); PIXIE: Kogut et al. (2011); PRISM: André et al. (2014)). It will open a window into the very beginning of our universe.

A major challenge of CMB B-mode detection is to accurately remove polarized galactic foregrounds (Planck Collaboration et al. 2015b,a,c). At CMB frequency of ~ 100 GHz, a major foreground is the galactic thermal dust, which likely dominates over CMB B-mode at $\nu \gtrsim 100$ GHz, even for the cleanest sky areas (BICEP2/Keck and Planck Collaborations et al. 2015). Synchrotron emission is another major foreground, especially at lower frequency. Other polarized foregrounds such as spinning dust (Planck Collaboration et al. 2011, 2015b) and magnetic dust (Draine & Hensley 2012; Planck Collaboration et al. 2015d) may also be non-negligible.

Usually CMB experiments rely on multi-frequency information to remove foregrounds (e.g. Planck Collaboration et al. (2015b,a,c); Kogut et al. (2011); André et al. (2014)). This kind of approaches faces various challenges. First, the exact frequency dependences of foregrounds and the exact number of independent foregrounds are unknown. Even worse, recently Planck found that dust foregrounds at 217 and 353 GHz bands are decorrelated at a few percent level, which may lead to a significant bias in r (tensor-to-scalar ratio) (Remazeilles et al. 2016; Planck Collaboration et al. 2016a; Poh & Dodelson 2016). To avoid such potential bias, alternative methods have been constructed (e.g. Tegmark et al. (2003); Delabrouille et al. (2003); Cardoso et al. (2008)) and applied (e.g. Planck Collaboration et al. (2015a)). For example, SMICA (Delabrouille et al. 2003; Cardoso et al. 2008) simultaneously fits many unknown parameters of CMB and foregrounds against the power spectrum measurements of all frequency bands and multipole bins. However, it is computationally highly challenging due to the large number of unknowns. When applied to data analysis such as Planck, various simplifications and assumptions are often made in parameter fitting (e.g. Planck Collaboration et al. (2015a)).

Here we report the **ABS** method, which stands for the **A**nalytical method of **B**lind **S**eparation of CMB from foregrounds. It can be treated as post-processing on the matrix of cross bandpower between frequency bands, which are heavily compressed products of original (noisy) maps. It works on any single multipole bin. Due to the fact that CMB B-mode has a known (blackbody) frequency dependence, a set of specific linear algebra operations on this measured matrix automatically returns the bandpower $\mathcal{D}_{\rm B}(\ell)$, the most important B-mode statistics. The measurement procedure is completely fixed by the measured matrix and survey specifications, with no assumptions on foregrounds. Since it does not rely on fitting procedures, it is numerically stable and superfast. All these are made possible by the analytical solution (Eq. 2) that we discover.

This paper is organized as follows. In §2 we describe the ABS method. In §3 we test the ABS method against simulated observations of various frequency configurations, instrumental noise and foregrounds. §4 provides a diagnostics for a planned survey to achieve unbiased B-mode measurement. We discuss and conclude in §5. The appendix contains proof of a few key results.

2. THE ABS METHOD

The ABS method is motivated by the analytical solution of $\mathcal{D}_{\rm B}$ derived under the ideal case of no instrument noise, which is then naturally extended to the case with

zhangpj@sjtu.edu.cn

instrumental noise.

2.1. *The analytical solution for the case of no instrument noise*

Our method works on $\mathcal{D}_{ij}(\ell)$, the $N_f \times N_f$ matrix of cross bandpower between the i-th and j-th frequency bands. Here $i, j = 1, 2 \cdots N_f$ and N_f is the number of frequencies. In thermodynamic units,

$$\mathcal{D}_{ij}(\ell) = f_i^{\rm B} f_j^{\rm B} \mathcal{D}_{\rm B}(\ell) + \mathcal{D}_{ij}^{\rm fore}(\ell) \ . \quad (1)$$

Since we use the thermodynamic units, $f^{\rm B} = 1$. $\mathcal{D}_{ij}^{\rm fore}$ is the cross bandpower matrix of foreground. It has order N_f, but its rank M depends on the number of independent foreground components. Our task is to solve Eq. 1 for $\mathcal{D}_{\rm B}(\ell)$ of a single multipole ℓ bin, without assumptions of $\mathcal{D}_{ij}^{\rm fore}$. This may appear as a mission impossible. However, due to two facts that $N_f \times N_f$ matrix $\mathcal{D}_{ij}$ has only $M+1$ eigenvectors and that $f^{\rm B}(\nu)$ is known, we are able to prove the following two key results.

- **The solution to $\mathcal{D}_{\rm B}$ is unique, as long as $M < N_f$.**
- **The analytical solution exists, given by**

$$\mathcal{D}_{\rm B} = \left(\sum_{\mu=1}^{M+1} G_\mu^2 \lambda_\mu^{-1} \right)^{-1} \ . \quad (2)$$

Here, the μ-th eigenvector of $\mathcal{D}_{ij}$ is $\mathbf{E}^{(\mu)}$, which has eigenvalue λ_μ and normalization $\mathbf{E}^{(\mu)} \cdot \mathbf{E}^{(\mu)} = 1$. The eigenmodes are always ranked with decreasing order in $|\lambda_\mu|$. Since $\mathcal{D}_{ij}$ is positive definite, $\lambda_\mu > 0$. $G_\mu \equiv \mathbf{f}^{\rm B} \cdot \mathbf{E}^{(\mu)}$. We prove the uniqueness of the solution and derive Eq. 2 in the appendix. Eq. 2 also proves the uniqueness of the solution.

Eq. 2 is not straightforward to understand. However, for the limiting case of $M \leq 2$, one can solve for all eigenmodes analytically and verify Eq. 2 by brute-force. This equation also confirms our instinct that any foreground components orthogonal to the CMB signal in the frequency space do not interfere the B-mode reconstruction.

2.2. *Natural extension to the case with instrument noise*

Instrument noise adds random noise $\delta\mathcal{D}_{ij}^{\rm inst}$ on the observed bandpower,

$$\mathcal{D}_{ij}^{\rm obs} \equiv \mathcal{D}_{ij} + \delta\mathcal{D}_{ij}^{\rm inst} \ . \quad (3)$$

Surprisingly, Eq. 2 can still be implemented in the data analysis, with straightforward modification to account for instrument noise.

- **Step 1**. We compute all N_f eigenmodes of $\mathcal{D}_{ij}^{\rm obs}$.
- **Step 2**. We measure $\mathcal{D}_{\rm B}$ from Eq. 2, *but only using eigenmodes with* $\lambda_\mu > \sigma_{\mathcal{D}}^{\rm inst}$.

Here $\sigma_{\mathcal{D}}^{\rm inst}$ is the r.m.s. of instrument noise in the bandpower. For brevity, we assume that all frequency bands have identical $\sigma_{\mathcal{D}}^{\rm inst}$.[1] Instrument noise not only affects physical eigenmodes, but also induces unphysical eigenmodes with eigenvalues of typical amplitude $\sigma_{\mathcal{D}}^{\rm inst}$. Therefore we exclude eigenmodes with $\lambda_\mu \leq \sigma_{\mathcal{D}}^{\rm inst}$. This selection criteria may not be optimal, but it already works well as we will show later.

The above method of measuring $\mathcal{D}_{\rm B}$, even including the determination of M, is completely fixed by the data, and relies on no priors of foregrounds.

Table 1
We test our ABS method against various CMB frequency configurations and instrumental noise. $\sigma_{\mathcal{D}}^{\rm inst}$ is the r.m.s. error in the bandpower measurement caused by instrumental noise.

Labels	frequency/GHz	$\sigma_{\mathcal{D}}^{\rm inst}/\mu{\rm K}^2$
S0	30, 70, 100, 150, 217 & 353	
S1	95, 150, 220 & 270	
S2	35, 95, 150, 220 & 270	
S3	35, 95, 150, 220, 270 & 353	$(10^{-5}, 10^{-2})$
S4	30, 36, 43, 51, 62, 75, 90,105, 135	
	160, 185,200, 220, 265, 300 & 320	

3. TESTING THE ABS METHOD

Next we test the ABS method against simulated $\mathcal{D}_{ij}^{\rm obs}$ with a variety of foregrounds, instrument noise and survey frequency configurations.

3.1. *Simulated observations*

To generate simulated $\mathcal{D}_{ij}^{\rm obs}$, we approximate $\delta\mathcal{D}_{ij}^{\rm inst}$ as Gaussian distributed with dispersion $\sigma_{\mathcal{D}}^{\rm inst}$. $\sigma_{\mathcal{D}}^{\rm inst}$ is a key factor in CMB B-mode search. BICEP2/Keck has reached $\sigma_{\mathcal{D}}^{\rm inst} \sim 10^{-3}\mu{\rm K}^2$ (BICEP2/Keck and Planck Collaborations et al. 2015). Future experiments can go well below $10^{-4}\mu{\rm K}^2$. For example, PRISM (André et al. 2014) has typical noise $\sim 70\mu{\rm K/detector/arcmin}^2$, ~ 200 detectors per band, $\sigma_{\mathcal{D}}^{\rm inst} \simeq 3.7 \times 10^{-5}\mu{\rm K}^2(\ell/\Delta\ell)^{1/2}(0.5/f_{\rm sky})^{1/2}(\ell/80)$. Here $\Delta\ell$ is the width of multipole bin and $f_{\rm sky}$ is the fractional sky coverage. Other experiments such as COrE, EPIC and LiteBIRD have similar sensitivity. We consider a wide range of $\sigma_{\mathcal{D}}^{\rm inst} \in (10^{-5}, 10^{-2})\mu{\rm K}^2$ to include all these possibilities.

Frequency configuration is crucial for foreground removal. We consider five configurations (**S**0-**S**4), shown in Table 1.

- **S**0 is the fiducial one, with 6 bands centered at 30, 70, 100, 150, 217 & 353 GHz. This configuration is similar to Planck. It has a wide frequency coverage, good for both radio and foreground removal.
- **S**1 has 4 bands at 95, 150, 220 & 270 GHz (Keck array-like, Grayson et al. (2016)). A major difference of **S**1 to **S**0 is the lack of low frequency bands and hence limited capability of radio foreground identification and removal.

[1] For realistic surveys, instrumental noise varies across frequency bands and the cut in step 2 should be replaced by some sort of average over $\sigma_{\mathcal{D}}^{\rm inst}$ of each band. For such situation, quantitative study has to target at each specific surveys. Since we do not expect fundamental impacts to our method, we leave such investigation in future works.

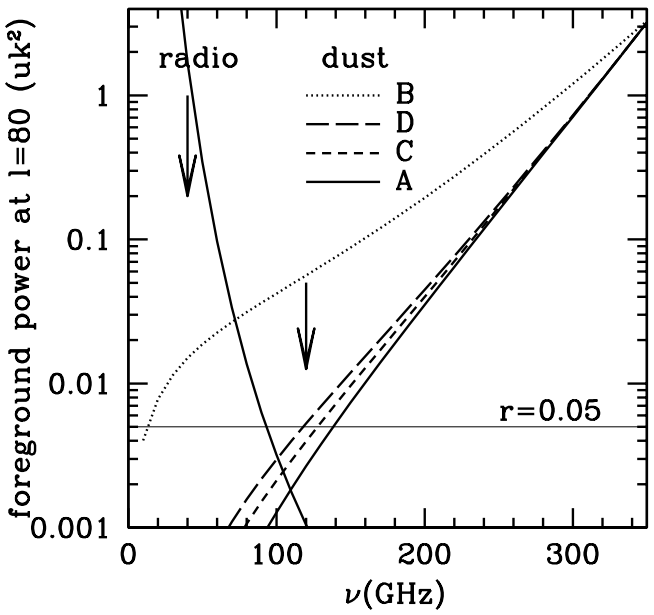

Figure 1. The simulated observation for testing our method is constructed adopting 4 foreground models. They share identical radio foreground, but different dust model parameters. Case C and D differ from case A and B by significant decorrelation between dust foregrounds at different frequencies. Case B and D are likely unrealistic and should be treated as extreme tests of our method.

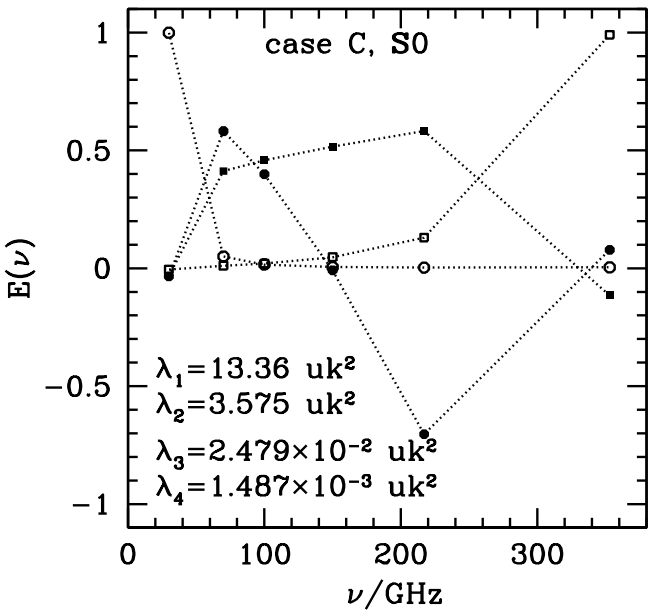

Figure 2. The eigenvectors and eigenvalues for foreground case C and frequency configuration **S**0 of $N_f = 6$ bands, with $\mathcal{D}_{\rm B} = 5 \times 10^{-3}\mu{\rm K}^2$ and centered at $\ell = 80$. Due to significant decorrelation of thermal dust foreground, case C has 4 eigenmodes. (1) The first eigenmode (open circle) is dominated by radio foreground, with eigenvalue λ_1 essentially its band power at 30 GHz. Since the radio model is actually the observational upper limit, this eigenmode may be much less significant in reality. (2) The second eigenmode (open square) is dominated by dust emission, with λ_2 essentially the dust emission band power at 353 GHz. (3) The third eigenmode (filled square) is dominated by CMB B-mode. (4) The fourth eigenmode (filled circle) is a mixture of all foreground and CMB components. Although it is subdominant, it has to be robustly identified for unbiased B-mode measurement, as detailed in Fig. 6.

- **S**2 adds a 35 GHz bands to **S**1 (BICEP array-like, Grayson et al. (2016)). This is to test the gain adding a low frequency band.
- **S**3 further adds a 353 GHz band to **S**2. This turns out to be important for dust foreground removal when decorrelation in dust foreground exists.
- **S**4 has 16 bands between 30 GHz and 320 GHz. This is basically the frequency configuration of PRISM (André et al. 2014), expect that PRISM also has higher frequency bands.

Simulating $\mathcal{D}_{ij}^{\rm obs}$ also requires $\mathcal{D}_{ij}$. For the signal, we focus on $\ell = 80$ around the recombination bump. The fiducial $\mathcal{D}_{\rm B} = 5 \times 10^{-3}\mu{\rm K}^2$, corresponding to the sum of $r = 0.05$ and the lensing B-mode. We also consider $\mathcal{D}_{\rm B} = 2 \times 10^{-3}\mu{\rm K}^2$ in which the lensing B-mode dominates. Tests around $\ell = 5$ of the reionization bump shows equally excellent performance.

For foregrounds, we specify $\mathcal{D}_{ij}^{\rm fore} = \sum_{\alpha=1}^{M} f_i^{(\alpha)} f_j^{\alpha)} \mathcal{D}_\alpha$. $f_i^{(\alpha)} \equiv f^{(\alpha)}(\nu_i)$ is the frequency dependence of the α-th foreground component and $\mathcal{D}_\alpha$ is the bandpower amplitude. Throughout the paper, we include two polarized foregrounds (galactic dust and galactic synchrotron). When we consider decorrelation between galactic dust at different frequency, we need at least two $f^\alpha(\nu)$ to describe dust alone. Therefore $M = 2$ if no decorrelation and $M \geq 3$ when decorrelation exists.

We consider four foreground models (case A, B, C, D, Fig. 1). They all share the same radio synchrotron foreground, *but different dust foregrounds*. For radio,

$$f^{\rm radio}(\nu) \propto \nu^{-\beta_{\rm R}/2} \frac{(e^x-1)^2}{e^x x^4} \ , \ \mathcal{D}_{\rm radio} \propto \ell^{-0.6} \ . \quad (4)$$

Here $\beta_{\rm R} = 3.3$ is the frequency index and $x \equiv h\nu/(k_B T_{\rm CMB})$. The bandpower is normalized as $3 \times 10^{-4}\mu{\rm K}^2$, at $\nu = 150$GHz and $\ell = 80$. This is the observationally allowed upper limit in the BICEP2 sky (BICEP2/Keck and Planck Collaborations et al. 2015).

For the galactic dust foreground, we adopt (Planck Collaboration et al. 2016b)

$$f^{\rm dust}(\nu) \propto \frac{x^{\beta_{\rm d}}(e^x-1)^2}{xe^x(e^{xT_{\rm CMB}/T_{\rm d}}-1)} \ , \ \mathcal{D}_{\rm dust} \propto \ell^{-0.42} \ . \quad (5)$$

To account for the recently detected decorrelation between different Planck frequency bands (Planck Collaboration et al. 2016a), we adopt a simple model of spatially stochastic variation in the dust index $\beta_{\rm d}$(Planck Collaboration et al. 2016a). It induces a new component in $\mathcal{D}_{ij}(\ell)$,

$$f^{\rm S}(\nu) = f^{\rm dust}(\nu) \times \ln(\nu/\nu_0) \ , \ \mathcal{D}_{\rm S} = \mathcal{D}_{\rm dust} A_{\rm S} \ . \quad (6)$$

Here we adopt $\nu_0 = 353$ GHz. $A_{\rm S} \propto \langle \delta\beta_{\rm d}^2 \rangle$ is a free parameter to control the level of decorrelation. When this stochastic component is subdominant, the cross correlation coefficient between dust in i-th and j-th bands is $\mathcal{R}^{\rm BB}_{\nu_i\nu_j} \simeq 1 - \frac{1}{2}A_{\rm S}(\ln(\nu_i/\nu_j))^2$. The overall bandpower is normalized as $3.5\mu{\rm K}^2$ at $\ell = 80$ and 353 GHz (BICEP2/Keck and Planck Collaborations et al. 2015).

We adopt 4 cases of dust parameters, $(\beta_{\rm d}, T_{\rm d}, A_{\rm S})$

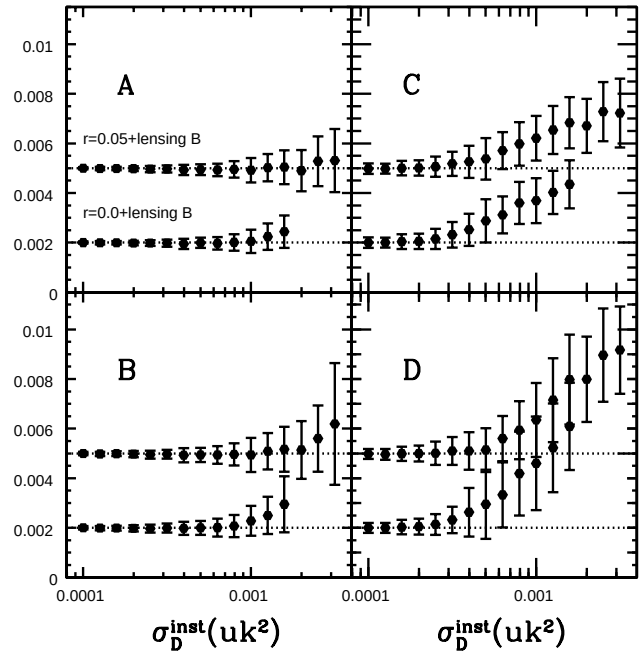

Figure 3. Tests for the **S**0 survey configuration and 4 cases of foregrounds. Dot lines are the input B-mode. Points are the output of our method and error bars are estimated using 100 realizations of instrument noise with r.m.s. $\sigma_{\mathcal{D}}^{\rm inst}$. The input $\mathcal{D}_{\rm B}$ is recovered unbiasedly when the instrumental noise is below certain thershold. Above this threshold, bias in $\mathcal{D}_{\rm B}$ develops. Such bias reflects the survey limitation of foreground removal, explained by Fig. 6. We emphasize that the adopted foreground cases are to generate simulated observational data. Our ABS method assumes nothing about these foregrounds.

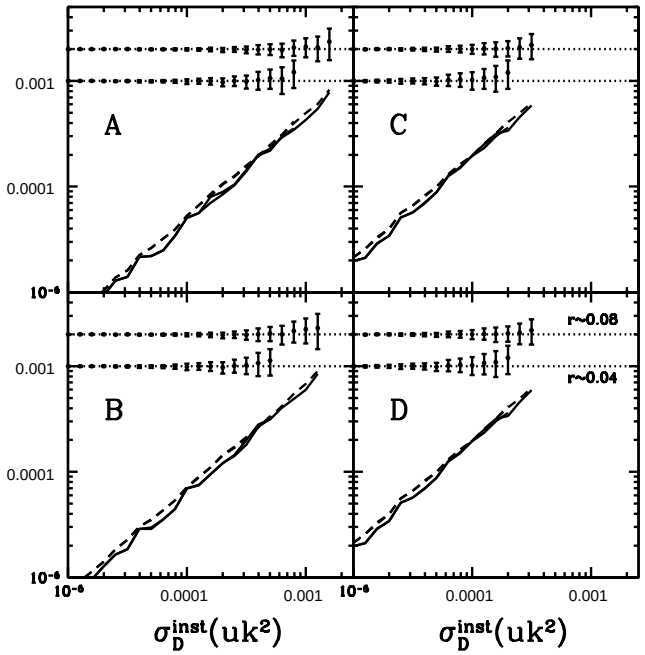

Figure 4. Similar to Fig. 3, but for $\ell = 5$ around the reionization bump. We also plot the errorbars as functions of $\sigma_{\mathcal{D}}$ (solid lines). Notice that statistical errors are insensitive to $\mathcal{D}_{\rm B}$. Therefore the two curves almost overlap. Furthermore, the prediction of Eq. 8 is plotted as dash lines, which agree with the numerical results well. Notice that, due to smaller B-mode at this scale and smaller instrumental noise (scales as ℓ^{-1}), we use different range of $\sigma_{\mathcal{D}}$ to that in Fig. 3.

$= (1.59, 19.6, 0.0)$, $(0.5, 10, 0.0)$, $(1.59, 19.6, 0.42)$, $(1.59, 19.6, 0.84)$. Case A is the best fit of Planck (Planck Collaboration et al. 2016b). Case B has a factor of 10 more dust contamination at 100-150 GHz than case A, and also a much flatter spectrum. Case C has dust decorrelation between frequency bands, reproducing the Planck finding of $\mathcal{R}^{BB}_{353,217} = 0.95$ (Planck Collaboration et al. 2016a). Case D has unrealistically large decorrelation (e.g. $\mathcal{R}^{BB}_{353,150} = 0.7$). Both case B and D serve as extreme tests of our method.

The eigenmodes of $\mathcal{D}_{ij}$ depend on foregrounds, CMB signal and observational frequency configuration. An useful relation to understand these eigenmodes is

$$\sum_\alpha \lambda_\alpha = {\rm Tr}\mathcal{D}_{ij} = \sum_i \mathcal{D}_{ii} \ . \qquad (7)$$

Fig. 2 shows the eigenmodes for foreground model C, $\mathcal{D}_{\rm B} = 5\times10^{-3}\mu{\rm K}^2$, and frequency configuration **S**0. Since it has significant decorrelation in dust foreground, it has 4 eigenmodes. The first two are essentially synchron and dust foreground, respectively. These can be seen from their frequency dependences (the shapes of eigenvectors). Furthermore, $\lambda_1 \simeq \sum_i \mathcal{D}^{\rm radio}_{ii} \sim \mathcal{D}^{\rm radio}_{11}$, $\lambda_2 \simeq \sum_i \mathcal{D}^{\rm dust}_{ii} \sim \mathcal{D}^{\rm dust}_{66}$. The third one is dominated by CMB, $\lambda_3 \simeq 5\mathcal{D}_{\rm B}$, close to $N_f\mathcal{D}_{\rm B} = 6\mathcal{D}_{\rm B}$ which is the limit of pure CMB B-mode. For the same reason, it contains non-negligible contamination from foregrounds. The fourth eigenmode is a mixture of CMB and foregrounds, with a frequency dependence resembling none of CMB and foregrounds. It is subdominant, even comparing to the third one. However, later we will show that this eigenmode is non-negligible for unbiased measurement of CMB B mode.

3.2. *Test results*

For the **S**0 frequency configuration, our method faithfully extracts the input B-mode, as long as the instrumental noise is below certain threshold $\sigma_{\mathcal{D}}^{\rm thres}$ (Fig. 3 at $\ell \sim 80$ & Fig. 4 at $\ell \sim 5$). When the instrumental noise is below certain threshold, the ABS method is unbiased and the statistical error $\sigma_{\mathcal{D}} \propto \sigma_{\mathcal{D}}^{\rm inst}$. We have also checked against other configurations and confirm that our method has the following advantages.

The recovered B-mode is insensitive to the overall amplitude and spectral shape of galactic foregrounds. For example, case B has a factor of ~ 10 larger dust contamination at ~ 150 GHz band than case A. It also has a much flatter spectrum. Both would severely degrade the CMB extraction. However, the performance is almost as good as case A, with statistical error just 40% larger. This insensitivity of the overall foreground amplitude is also confirmed against tests at $\ell \sim 5$ around the reionization bump (Fig. 4), where the B-mode to foreground ratio is a factor of $\gtrsim 10$ smaller than at $\ell \sim 80$.

Furthermore, our ABS method also works when decorrelation of foregrounds at different frequencies exists (case C & D, Fig. 3 & 4). Case C & D have one more foreground component, but our method nevertheless recovers the input B-mode, robustly and blindly. This demonstrates the advantage that the ABS method needs no assumptions on the number of independent foreground

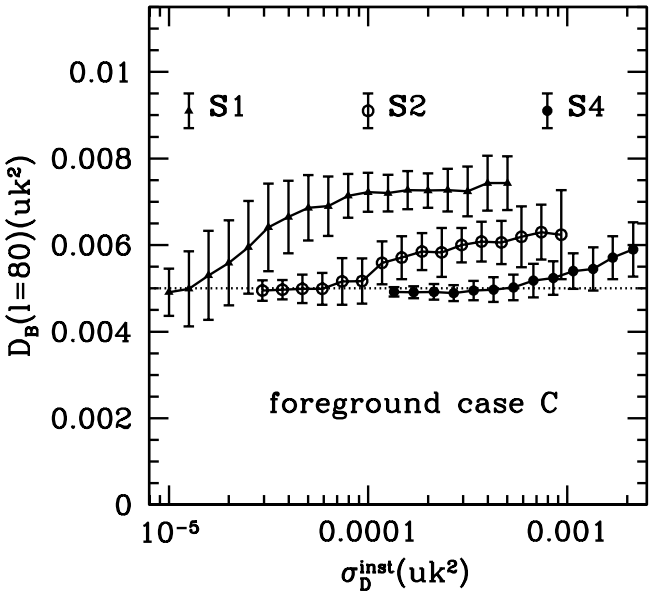

Figure 5. The impact of frequency coverage on B-mode extraction. The result of **S**3 falls between **S**2 and **S**4 and for clarity is not shown. Incomplete frequency coverage fails to identify certain eigenmodes significant for B-mode measurement (Fig. 6) and causes bias in $\mathcal{D}_{\rm B}$.

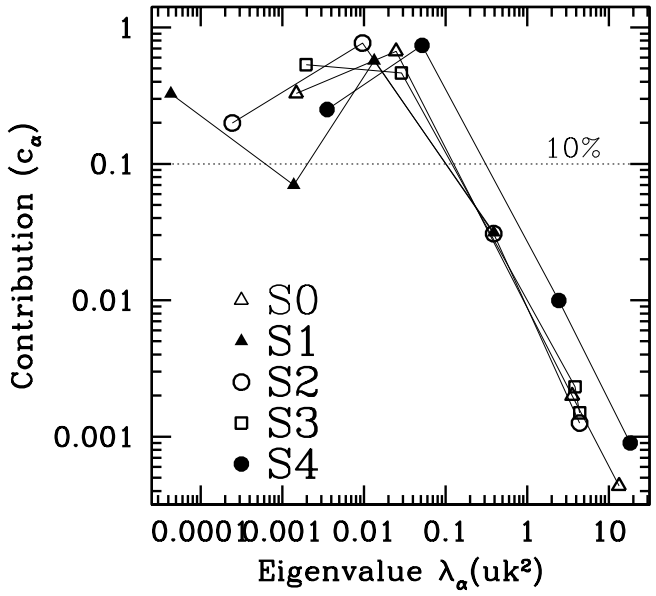

Figure 6. A diagnostic of unbiased B-mode extraction. If $\lambda_\alpha \lesssim \sigma_{\mathcal{D}}^{\rm inst}$, instrument noise messes up this physical eigenmode. Missing it results in a fractional systematic error of $\sim c_\alpha/(1-c_\alpha)$ in $\mathcal{D}_{\rm B}$, explaining the biases observed in Fig. 3 & 5.

components. The price to pay is a factor of ~ 4 larger statistical error (e.g. case C/D vs. case A/B). For case C and D, the statistical error is $\sim 2\sigma_{\mathcal{D}}^{\rm inst}$ in the limit $\sigma_{\mathcal{D}}^{\rm inst} \to 0$. This is a factor of 5 larger than the instrument sensitivity ($\sigma_{\mathcal{D}}^{\rm inst}/\sqrt{N_f}$). This result cautions that we should not simply use the instrument sensitivity as the lower limit of CMB B-mode detection, given complexities in foregrounds.

Another advantage of our method is its numerical stability. Each error-bar shown in Fig. 3 & 4 is estimated using 100 realizations of $\delta\mathcal{D}_{ij}^{\rm inst}$, among which we find no blow up of our method when $\sigma_{\mathcal{D}}^{\rm inst} < \sigma_{\mathcal{D}}^{\rm thres}$. Furthermore, the estimated errors agree well with the analytical result of perturbing Eq. 2, as derived in the appendix C,

$$\sigma_{\rm B} = \sqrt{2}\sigma_{\mathcal{D}}^{\rm inst}\left(\sum_{\mu=1}^{M+1}\frac{G_\mu^2}{\lambda_\mu^2}\right)\mathcal{D}_{\rm B}^2 \ . \qquad (8)$$

This agreement further shows the numerical stability of our method against instrument noise, even though the $1/\lambda_\mu$ operation in Eq. 2 may look scary.

4. TOWARDS UNBIASED MEASUREMENT

Nevertheless, when instrument noise $\sigma_{\mathcal{D}}^{\rm inst}$ exceeds certain threshold ($\sigma_{\mathcal{D}}^{\rm thres}$), systematic bias develops in the extracted $\mathcal{D}_{\rm B}$. It is always positive, increases with $\sigma_{\mathcal{D}}^{\rm inst}$ until reaching a plateau. Why does $\sigma_{\mathcal{D}}^{\rm thres}$ exist? What determines its value? What causes the general dependence of bias on $\sigma_{\mathcal{D}}^{\rm inst}$? It turns out that the induced bias is a combined consequence of foregrounds and survey frequency configurations. It is well understood within the frame of the ABS method, and actually reflects the limitation of a given CMB experiment to cleanly remove foregrounds.

For the **S**0 frequency configuration, the induced bias is most significant when decorrelation exists (case C and D, when $\sigma_{\mathcal{D}}^{\rm inst} \gtrsim 10^{-3}\mu{\rm K}^2$). For **S**1, the situation worsens severely. Even for instrument noise as low as $\sigma_{\mathcal{D}}^{\rm inst} = 10^{-4}\mu{\rm K}^2$, a systematic error of 40% of the signal and 5 times of the statistical error shows up (Fig. 5, for case C). Adding a 35 GHz band (the **S**2 configuration) can significantly reduce this systematic error. But it again reaches $\sim 2\sigma$ when $\sigma_{\mathcal{D}}^{\rm inst} \gtrsim 3\times10^{-4}\mu{\rm K}^2$. Further adding a 353 band (the **S**3 configuration), the systematic error disappears until $\sigma_{\mathcal{D}}^{\rm inst} \gtrsim 10^{-3}\mu{\rm K}^2$. The **S**0 configuration shares similar behavior as **S**3 (Fig. 3). Adding more frequency bands (**S**4) further reduces the systematic error.

These systematic errors do not reflect flaws in our method, since they are caused by the survey limitation of foreground removal. Our methodology provides a specific diagnostic for this survey limitation. Eq. 2 defines the contribution of each eigenmode to the measurement of $\mathcal{D}_{\rm B}$,

$$c_\alpha \equiv \frac{G_\alpha^2/\lambda_\alpha}{\sum_{\mu=1}^{M+1} G_\mu^2/\lambda_\mu} \ . \qquad (9)$$

The necessary condition of unbiased $\mathcal{D}_{\rm B}$ measurement by a given survey is that all eigenmodes of significant c_α must be robustly identified ($\lambda_\alpha \gg \sigma_{\mathcal{D}}^{\rm inst}$). Missing the α-th eigenmode, for which both large instrument noise and incomplete frequency coverage can be responsible, will bias the extracted $\mathcal{D}_{\rm B}$ by a fraction

$$\frac{\delta\mathcal{D}_{\rm B}}{\mathcal{D}_{\rm B}} \simeq \frac{c_\alpha}{1-c_\alpha} \ . \qquad (10)$$

Since λ_α is positive, c_α is positive. Therefore missing the

α-th eigenmode causes overestimation of $\mathcal{D}_{\rm B}$.

Instrument noise messes up physical eigenmodes with $\lambda_\alpha \lesssim \sigma_{\mathcal{D}}^{\rm inst}$. Incomplete frequency coverage has poor capability of separating foregrounds and CMB in frequency space. It causes the existence of some eigenmodes with significant c_α but tiny λ_α.

Fig. 6 shows λ_α-c_α in the **S**0-**S**4 configurations, for case C and $\mathcal{D}_{\rm B} = 5\times10^{-3}\mu{\rm K}^2$. $\mathcal{D}_{ij}$ of case C has $M+1=4$ physical eigenmodes. The first two are usually dominated by foregrounds and therefore have large eigenvalues. But due to the $1/\lambda_\mu$ weighting in Eq. 2, their impacts on the B-mode extraction are automatically suppressed to a level negligible ($c_\alpha \ll 1$) . Usually both the third and fourth eigenmodes have significant c_α, and therefore are important for B-mode extraction. The problem of **S**1 is that the fourth eigenmode has a large $c_4 = 0.33$ but a tiny $\lambda_4 = 4.3\times10^{-5}\mu{\rm K}^2$. Missing it biases $\mathcal{D}_{\rm B}$ high by $\sim c_4/(1-c_4) = 50\%$. This explains the large bias found in **S**1, where $\sigma_{\mathcal{D}}^{\rm inst} \gtrsim \lambda_4$ (Fig. 5).

Adding the 35 GHz band (**S**2) improves the identification of radio foreground and pushes $\lambda_4 = 2.4\times10^{-4}\mu{\rm K}^2$, with $c_4 = 0.2$. This significantly improves the situation, until $\sigma_{\mathcal{D}}^{\rm inst} \gtrsim \lambda_4$, where a bias of $c_4/(1-c_4) \simeq 25\%$ develops. An extra 353 GHz band pushes all $\lambda_\alpha > 10^{-3}\mu{\rm k}^2$ and further improves the situation (**S**3, **S**4 & **S**0). Adding more frequency bands further reduces the bias (**S**1→**S**4), for fixed $\sigma_{\mathcal{D}}^{\rm inst}$.

Future experiments such as COrE, PRISM and PIXIE will have dozens or more frequency bands, and low instrument noise ($\sigma_{\mathcal{D}}^{\rm inst} \lesssim 10^{-4}\mu{\rm K}^2$). Such high degree of redundancy would make them safe for even more complicated foregrounds. We expect them to achieve unbiased and precise measurement of $\mathcal{D}_{\rm B}$ (e.g. **S**4, Fig. 5).

5. CONCLUSION AND DISCUSSION

Our test considers both synchrotron and thermal dust foreground and takes decorrelation of dust foreground into account. However, we have not considered other possible foregrounds such as spinning dust, due to large uncertainty in their understandings. In future works we plan to include more foregrounds, consider more realistic (and therefore more complicated) instrumental noise, and redo the tests carried out in this paper. Nevertheless, since our method makes no assumption on foreground, it is expected to work with the existence of foregrounds other than synchrotron and thermal dust foregrounds.

Our ABS method applies when survey windows/masks exist. There are two options. One is to pre-process each map to have identical windows/masks first. One then takes the convolved $\mathcal{D}_{ij}^{\rm obs}$ as input and measures the convolved $\mathcal{D}_{\rm B}$ using the ABS method. One then deconvolves to obtain the true B-mode. The other possibility is to deconvolve the survey window of each map and measure the deconvolved $\mathcal{D}_{ij}^{\rm obs}$ first and then apply the ABS method. The problem of the second approach is that imperfectness of deconvolution of each map may cause $f_i^{\rm B} \neq 1$. Unless we can figure out the value of $f_i^{\rm B}$ for each band, the B-mode measurement will be biased. For such reason, the first approach is likely safter, and meanwhile more straightforward.

We then conclude that our method is applicable to general case of foregrounds for blind, yet accurate, extraction of CMB B-mode. It is also numerically stable against various instrument noise. It further provides a quantitative requirement (Eq. 9) for unbiased B-mode measurement, useful for design of future CMB experiments.

Our ABS method is distinctively different to SMICA, other than sharing an identical goal to solve Eq. 1 for $\mathcal{D}_{\rm B}$. (1) To our best knowledge, this is the first time that the analytical solution (Eq. 2) is discovered and the analytical B-mode extraction method based on it is constructed. It avoids the delicate multi-parameter fitting in SMICA, which is time consuming and is often numerically challenging. (2) The SMICA algorithm is based on the Gaussian assumption for all components and noise, which may be invalid in the real-world circumstance. In contrast, our method makes no such assumption, making it unbiased to lensing B-mode. (3) A key requirement of SMICA is constant $f^{(\alpha)}$ over ℓ bins. In contrast, our method works on individual ℓ bin. It does not need such assumption at all and therefore is applicable to more general foregrounds.

Our method also works for blind measurements of CMB spectra distortion, E-mode polarization and the thermal SZ effect. Furthermore, it has important applications even in totally different areas. For example, it may serve as the ultimate solution to the original proposal of extracting cosmic magnification by counting galaxies (Zhang & Pen 2005). This ongoing project[2] extends and will supersedes previous works (Zhang & Pen 2005; Yang et al. 2015) Given its excellent performance, other potential applications should be explored too.

6. ACKNOWLEDGMENTS

We thank Xuelei Chen, Xinjuan Yang and Yu Yu for useful discussions. This work was supported by the National Science Foundation of China (11273018, 11433001, 11320101002) and National Basic Research Program of China (2015CB857001, 2013CB834900).

APPENDIX

UNIQUENESS OF SOLUTION

We first define vectors in frequency space of N_f dimensions, $\mathbf{f}^{(\alpha)} \equiv (f_1^{(\alpha)}, \cdots, f_{N_f}^{(\alpha)})$. Without loss of generality, we absorb $\mathcal{D}_\alpha$ into corresponding $\mathbf{f}^{(\alpha)}$. Suppose that $(\sigma, \mathbf{h}^{(1)}, \cdots, \mathbf{h}^{(M)})$ is also a set of solution to Eq. 1,

$$\mathcal{D}_{ij} = f_i^{\rm B} f_j^{\rm B}\sigma + \sum_{\beta=1}^{M} h_i^{(\beta)} h_j^{(\beta)} \ . \tag{A1}$$

[2] X. Yang, J. Zhang, Y. Yu & P. Zhang, 2016, in preparation

Then, $\mathbf{h}^{(\beta)}$ must be linear combinations of the eigenvector $\mathbf{E}$s. Since $\mathbf{E}$s are linear combinations of vector $\mathbf{f}^{(\alpha)}$ and $\mathbf{f}^{\rm B}$, $\mathbf{h}^{(\beta)}$ must be linear combinations of $\mathbf{f}^{(\alpha)}$ and $\mathbf{f}^{\rm B}$,

$$\mathbf{h}^{(\beta)} = \left[\sum_{\alpha=1}^{M} R_{\alpha\beta}\mathbf{f}^{(\alpha)}\right] + B_\beta \mathbf{f}^{\rm B} \ . \tag{A2}$$

Here, $R_{\alpha\beta}$ and B_β are constants to be determined. Plug the above relation into Eq. A1 and compare against Eq. 1, we obtain

$$\begin{aligned} \sum_\beta R_{\alpha\beta}R_{\gamma\beta} &= \delta_{\alpha\gamma} \ , \\ \sum_\beta R_{\alpha\beta}B_\beta &= 0 \ , \\ \mathcal{D}_{\rm B} - \sum_\beta B_\beta^2 &= \sigma \ . \end{aligned} \tag{A3}$$

The first relation state that the matrix $\mathbf{R}$ is orthogonal, $\mathbf{R}^T\mathbf{R} = I$ where I is the unity matrix. Hence det$\mathbf{R} = \pm 1$. Therefore

$$\det\mathbf{R} \neq 0 \ \& \ \mathbf{R}\cdot\mathbf{B} = 0 \Rightarrow \mathbf{B} = 0 \Rightarrow \sigma = \mathcal{D}_{\rm B} \ . \tag{A4}$$

We then prove that the solution to $\mathcal{D}_{\rm B}$ is unique.

In contrast, solutions to $\mathbf{f}^{(\alpha)}$ are not unique, subject to transformation defined by $\mathbf{R}$ with det $\mathbf{R} = \pm 1$. Actually when det $\mathbf{R} = 1$, $\mathbf{R}$ is the unitary rotation matrix operating in the M dimension frequency space. It is only after we fix the physics of each $\mathbf{f}$s, may we uniquely solve them.

ANALYTICAL SOLUTION OF $\mathcal{D}_{\rm B}$

From Eq. 1, we obtain $E_{\mu\nu} = G_\mu G_\nu \mathcal{D}_{\rm B} + F_{\mu\nu}$. Here, $F_{\mu\nu} \equiv \sum_{ij} E_i^{(\mu)} \mathcal{D}_{ij}^{\rm fore} E_j^{(\nu)}$ and $G_\mu \equiv \sum_i f_i^{\rm B} E_i^{(\mu)}$. $E_{\mu\nu}$ is diagonal ($E_{\mu\nu} = \lambda_\mu \delta_{\mu\nu}$), with order $M+1$ and rank $M+1$. Moving $G_\mu G_\nu \mathcal{D}_{\rm B}$ to the l.h.s., we obtain

$$E_{\mu\nu} - G_\mu G_\nu \mathcal{D}_{\rm B} = F_{\mu\nu} \ . \tag{B1}$$

The rank of $\mathbf{F}$ is M, smaller than its order $M+1$. As a result,

$$\det\left(E_{\mu\nu} - G_\mu G_\nu \mathcal{D}_{\rm B}\right) = 0 \ . \tag{B2}$$

The Sylvester's determinant theorem states that for matrices A $(m\times n)$, B$(n\times m)$, X$(m\times m)$ and unitary matrix I_n $(n\times n)$,

$$\det(\mathbf{X} + \mathbf{AB}) = \det(\mathbf{X})\det(\mathbf{I}_n + \mathbf{BX}^{-1}\mathbf{A}) \ . \tag{B3}$$

Eq. B2 then becomes

$$0 = \det\left(\mathbf{E} - \mathbf{G}\mathbf{G}^T\mathcal{D}_{\rm B}\right) = \det(\mathbf{E})(1 - \mathcal{D}_{\rm B}\mathbf{G}^T\mathbf{E}^{-1}\mathbf{G}) \ .$$

Since $\det(\mathbf{E}) \neq 0$, we prove Eq. 2. It also proves the uniqueness of the solution for $\mathcal{D}_{\rm B}$ from Eq. 1.

THE ERROR ESTIMATION

The measured band powers are subject to instrumental noise. After subtracting the ensemble average from the diagonal elements, there will still be random noise $\delta\mathcal{D}_{ij}^{\rm inst}$ (with $\langle\delta\mathcal{D}_{ij}^{\rm inst}\rangle = 0$) on top of $\mathcal{D}_{ij}$ of Eq. 1. In the limit of small perturbations,

$$\delta\lambda_\mu = \delta\mathcal{D}_{\mu\mu} \ , \ \delta\mathbf{E}^{(\mu)} = \sum_{\nu\neq\mu} \frac{\delta\mathcal{D}_{\mu\nu}}{\lambda_\mu - \lambda_\nu}\mathbf{E}^{(\nu)} \ . \tag{C1}$$

Here $\delta\mathcal{D}_{\mu\nu} \equiv \sum_{ij} E_i^{(\mu)} \delta\mathcal{D}_{ij}^{\rm inst} E_j^{(\nu)}$. Correspondingly,

$$\delta G_\mu = \sum_{\nu\neq\mu} \frac{\delta\mathcal{D}_{\mu\nu}}{\lambda_\mu - \lambda_\nu} G_\nu \ , \ \delta E_{\mu\nu} = \delta\lambda_\mu\delta_{\mu\nu} \ .$$

Here we have required the eigenvectors to be normalized to unity, and for that, $E_{\mu\nu} = \lambda_\mu\delta_{\mu\nu}$. We obtain by perturbing Eq. 2,

$$\frac{\delta\mathcal{D}_{\rm B}}{\mathcal{D}_{\rm B}^2} = -\sum_\mu (2\delta G_\mu \lambda_\mu^{-1} G_\mu - \lambda_\mu^{-2}\delta\lambda_\mu G_\mu^2) = -\sum_\mu \sum_{\nu\neq\mu} \frac{2\delta\mathcal{D}_{\mu\nu}G_\mu G_\nu}{(\lambda_\mu - \lambda_\nu)\lambda_\mu} + \sum_\mu \lambda_\mu^{-2}\delta\mathcal{D}_{\mu\mu}G_\mu^2 \ . \tag{C2}$$

We now symmetrize the first term on the right side of the above equation. We can switch between $\mu \leftrightarrow \nu$ and take the average,

$$\frac{1}{2}\left(-\sum_{\mu}\sum_{\nu\neq\mu}\frac{2\delta\mathcal{D}_{\mu\nu}G_\mu G_\nu}{(\lambda_\mu-\lambda_\nu)\lambda_\mu}-\sum_{\nu}\sum_{\mu\neq\nu}\frac{2\delta\mathcal{D}_{\mu\nu}G_\mu G_\nu}{(\lambda_\nu-\lambda_\mu)\lambda_\nu}\right)=\sum_{\mu,\nu\neq\mu}\frac{\delta\mathcal{D}_{\mu\nu}G_\mu G_\nu}{\lambda_\mu\lambda_\nu}\ . \tag{C3}$$

Therefore

$$\frac{\delta\mathcal{D}_{\rm B}}{\mathcal{D}_{\rm B}^2}=\sum_{\mu,\nu}\frac{\delta\mathcal{D}_{\mu\nu}G_\mu G_\nu}{\lambda_\mu\lambda_\nu}\ . \tag{C4}$$

Notice that now the sum includes $\mu=\nu$ pairs. Eq. 8 can then be derived using the following relation,

$$\langle\delta\mathcal{D}_{\mu\nu}\delta\mathcal{D}_{\rho\sigma}\rangle=\sum_{ijkm}E_i^{(\mu)}E_j^{(\nu)}E_k^{(\rho)}E_m^{(\sigma)}\langle\delta\mathcal{D}_{ij}\delta\mathcal{D}_{km}\rangle=\sum_{ij}E_i^{(\mu)}E_j^{(\nu)}\sigma^{\rm inst}_{\mathcal{D},i}\sigma^{\rm inst}_{\mathcal{D},j}(E_i^{(\rho)}E_j^{(\sigma)}+E_i^{(\sigma)}E_j^{(\rho)})=\sigma^{\rm inst,2}_{\mathcal{D}}(\delta_{\mu\rho}\delta_{\nu\sigma}+\delta_{\mu\sigma}\delta_{\nu\rho})\ .$$

The second expression uses the relation

$$\langle\delta\mathcal{D}_{ij}\delta\mathcal{D}_{km}\rangle=\sigma^{\rm inst}_{\mathcal{D},i}\sigma^{\rm inst}_{\mathcal{D},j}\left[\delta_{ik}\delta_{jm}+\delta_{im}\delta_{jk}\right]\ .$$

REFERENCES

André, P., Baccigalupi, C., Banday, A., et al. 2014, JCAP, 2, 006
BICEP2 Collaboration, Ade, P. A. R., & et al. 2014, Physical Review Letters, 112, 241101
BICEP2/Keck and Planck Collaborations, Ade, P. A. R., Aghanim, N., et al. 2015, Physical Review Letters, 114, 101301
Bock, J., Cooray, A., Hanany, S., et al. 2008, ArXiv e-prints, arXiv:0805.4207
Cardoso, J.-F., Le Jeune, M., Delabrouille, J., Betoule, M., & Patanchon, G. 2008, IEEE Journal of Selected Topics in Signal Processing, 2, 735
Delabrouille, J., Cardoso, J.-F., & Patanchon, G. 2003, MNRAS, 346, 1089
Draine, B. T., & Hensley, B. 2012, ApJ, 757, 103
Gandilo, N. N., Ade, P. A. R., Benford, D., et al. 2016, ArXiv e-prints, arXiv:1607.06172
Grayson, J. A., Ade, P. A. R., Ahmed, Z., et al. 2016, ArXiv e-prints, arXiv:1607.04668
Inoue, Y., et al. 2016, arXiv:1608.03025
Kamionkowski, M., Kosowsky, A., & Stebbins, A. 1997, Physical Review Letters, 78, 2058
Keisler, R., Hoover, S., Harrington, N., et al. 2015, ApJ, 807, 151
Kogut, A., Fixsen, D. J., Chuss, D. T., et al. 2011, JCAP, 7, 025
Matsumura, T., Akiba, Y., Borrill, J., et al. 2014, Journal of Low Temperature Physics, 176, 733
Planck Collaboration, Ade, P. A. R., Aghanim, N., et al. 2011, A&A, 536, A20
Planck Collaboration, Adam, R., Ade, P. A. R., et al. 2015a, ArXiv e-prints, arXiv:1502.05956
—. 2015b, ArXiv e-prints, arXiv:1502.01588
Planck Collaboration, Ade, P. A. R., Aghanim, N., et al. 2015c, ArXiv e-prints, arXiv:1506.06660
Planck Collaboration, Ade, P. A. R., Alves, M. I. R., et al. 2015d, A&A, 576, A107
Planck Collaboration, Aghanim, N., Ashdown, M., et al. 2016a, ArXiv e-prints, arXiv:1606.07335
Planck Collaboration, Adam, R., Ade, P. A. R., et al. 2016b, A&A, 586, A133
Poh, J., & Dodelson, S. 2016, ArXiv e-prints, arXiv:1606.08922
Remazeilles, M., Dickinson, C., Eriksen, H. K. K., & Wehus, I. K. 2016, MNRAS, 458, 2032
Seljak, U. 1997, ApJ, 482, 6
Seljak, U., & Zaldarriaga, M. 1997, Physical Review Letters, 78, 2054
Starobinskii, A. A. 1979, Soviet Journal of Experimental and Theoretical Physics Letters, 30, 682
Tegmark, M., de Oliveira-Costa, A., & Hamilton, A. J. 2003, Phys. Rev. D, 68, 123523
The COrE Collaboration, Armitage-Caplan, C., Avillez, M., et al. 2011, ArXiv e-prints, arXiv:1102.2181
Thornton, R. J., Ade, P. A. R., Aiola, S., et al. 2016, ArXiv e-prints, arXiv:1605.06569
Yang, X., Zhang, P., Zhang, J., & Yu, Y. 2015, MNRAS, 447, 345
Zhang, P., & Pen, U.-L. 2005, Physical Review Letters, 95, 241302